

## Article

# Experimental Performance Study of Solar-Assisted Enhanced Vapor Injection Air-Source Heat Pump System

Zhengrong Li <sup>1</sup>, Yongheng Du <sup>1,2,\*</sup>, Yuqin Pan <sup>2</sup>, Fan Zhang <sup>3</sup>, Zhaofeng Meng <sup>3,\*</sup> and Yanan Zhang <sup>2</sup><sup>1</sup> School of Mechanical Engineering, Tongji University, Shanghai 200092, China<sup>2</sup> Henan Provincial Academy of Building Research Co., Ltd., Zhengzhou 450053, China<sup>3</sup> School of Energy and Environmental, Zhongyuan University of Technology, Zhengzhou 450007, China

\* Correspondence: hn\_dyh@tongji.edu.cn (Y.D.); mengzz@zut.edu.cn (Z.M.)

**Abstract:** In this paper, a solar-assisted enhanced vapor injection air-source heat pump (SC-EVIHP) system was built to investigate its heating performance in cold regions. A typical-weather day in Harbin was selected for the experiment, and the heating characteristics of the SC-EVIHP system were explored under variable working conditions. The experimental results showed that the system was greatly affected by solar radiation intensity. On typical-weather days in winter, the maximum values for the heating capacity and COP of the system appeared at the time of maximum radiation intensity. Compared with conventional enhanced vapor injection air-source heat pump systems (EVI-ASHPs), the heating capacity and COP were increased by 24.9% and 12.5% at most, respectively. The COP of the system increased by at most 11.1% under conditions where the outdoor temperature was  $-12\text{ }^{\circ}\text{C}$  and the outlet hot air temperature of the solar air collector was  $40\text{ }^{\circ}\text{C}$ . The SC-EVIHP system works well in a low-temperature environment and can be widely applied in cold regions.

**Keywords:** air-source heat pump; solar-air collector; enhanced vapor injection; COP



**Citation:** Li, Z.; Du, Y.; Pan, Y.; Zhang, F.; Meng, Z.; Zhang, Y. Experimental Performance Study of Solar-Assisted Enhanced Vapor Injection Air-Source Heat Pump System. *Energies* **2022**, *15*, 7730. <https://doi.org/10.3390/en15207730>

Academic Editor: Gianpiero Colangelo

Received: 19 September 2022

Accepted: 17 October 2022

Published: 19 October 2022

**Publisher's Note:** MDPI stays neutral with regard to jurisdictional claims in published maps and institutional affiliations.



**Copyright:** © 2022 by the authors. Licensee MDPI, Basel, Switzerland. This article is an open access article distributed under the terms and conditions of the Creative Commons Attribution (CC BY) license (<https://creativecommons.org/licenses/by/4.0/>).

## 1. Introduction

Heat pumps can absorb a large amount of low-grade heat energy in the external environment. Heat pumps are also energy-efficient, green and renewable, and easy to use as well as low-cost in installation, which make them easy to widely utilize and apply [1,2]. However, with a reduction in outdoor temperature, the heating capacity and COP of air-source heat pump (ASHP) systems drop sharply. This factor makes the heat pump difficult to promote in low-temperature areas [3–7].

Scholars at home and abroad have proposed different solutions to the limitations of ASHP systems. Jie et al. [8] experimentally found that by installing a flash tank, the exhaust temperature could be effectively reduced, which improved the reliability of the system in a low-temperature environment. Han et al. [9] went through comparative experiments and found that the performance of an ASHP system with vapor injection technology had obvious advantages compared with the conventional ASHP system under low-temperature conditions when the optimal injection ratio was achieved. Wei et al. [10] found that the defrosting efficiency of the ASHP system with vapor injection technology could be improved by 6.22% when the branch expansion valve was adjusted to the optimal opening. In summary, the running performance of an ASHP system with vapor injection technology is markedly improved compared with the conventional ASHP system. Heo et al. [11] proposed the optimal circulation control method by analyzing three different forms of vapor injection systems. For the heating capacity of the system, the optimal sub-cooler pressure ratio was suggested to be 0.4 to 0.7, and for the COP of the system, the optimal sub-cooler pressure ratio was suggested to be 0.7 to 0.8. Wang et al. [12] analyzed the performance of an ASHP system with a flash tank and a sub-cooler, respectively. They found that the ASHP system with a flash tank performed better. Li et al. [13] compared the effects of upstream and downstream injection on the performance of the heat pump system.

The results showed that downstream injection resulted in better operational performance. In summary, there are optimal operating conditions for an ASHP system using vapor injection technology. Superior performance of the system is significant under optimal operating conditions.

In recent years, with the increasing demand for clean energy, the application of solar systems has attracted the attention of many scholars. Jia et al. [14] proposed a CHP system based on a solar gas-assisted thermo-photovoltaic (TPV) device. It was found that the addition of solar energy could not only increase the output power of the TPV system but also could save a significant amount of fuel. Wang et al. [15] established a combined solar and gas-fired boiler heating system. It was found that the combined heating system had a clear advantage with respect to both energy savings and economics over gas-fired boiler capacity expansion. Aligholami et al. [16] established a solar chimney power plant model. It was found that a hydrophobic surface could improve the system performance by 11%. According to the above academic research, combined solar systems can achieve the effect of improving system performance, saving energy, and protecting the environment.

With the development of combined solar systems, the combined application of solar and heat pump systems has attracted the attention of many scholars wanting to improve the performance of heat pump systems. Yang et al. [17] simulated a solar-assisted air-source heat pump using models of serial, parallel, and dual-source indirect expansion. The results illustrated that the three heat pumps had the potential to be applied in areas with relatively low solar radiation intensity. Wang et al. [18] found through theoretical analysis that the combined operation of solar and ASHP systems could compensate for the shortcomings of the ASHP system. The overall stability of the combined system operation as well as the economic benefits were better. Long et al. [19] simulated the energy efficiency of the combined system during the cold season and showed that the combined system could achieve high-efficiency energy conservation by adjusting system connections according to meteorological conditions. Xu et al. [20] found that air flowing through the outdoor evaporator after being heated by the collector could improve the heat production and efficiency of the ASHP system. Karolis et al. [21] explored the system performance using a TRNSYS software simulation and the results showed that solar-assisted ASHP systems had significant advantages.

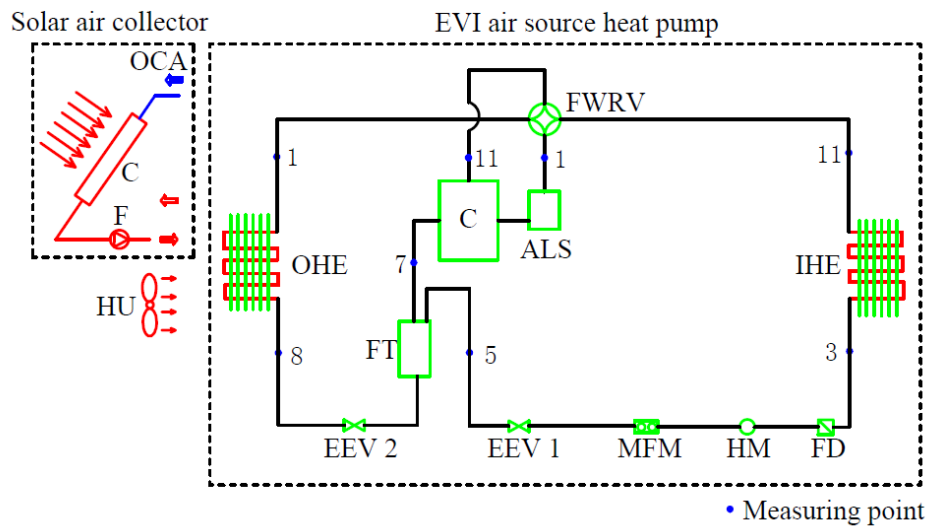
Research has shown that the COP and heating capacity of the EVI-ASHP system under low-temperature environmental conditions have been improved to a certain extent compared with the conventional ASHP system. However, further improvement of thermodynamic performance is also an urgent problem to be solved. A combined solar energy and EVI-ASHP system can improve operational performance. In this paper, this combined system was studied. The hot air heated by the solar air collector was directly blown to the air intake of the outdoor unit of the EVI-ASHP system, increasing the evaporation temperature of the heat pump in order to optimize the performance of the system. In our experimental analysis, the operational regulations of the system were explored so as to find the best operation scheme suitable for winter heating in cold areas and to provide experimental data as a basis for follow-up projects.

## 2. Experimental System and Theoretical Analysis

### 2.1. Test Device

The SC-EVIHP system was composed of two parts: a solar air collector and an EVI-ASHP system. The EVI-ASHP system included outdoor and indoor units. The outdoor unit included a compressor, four-way reversing valve, outdoor heat exchanger, electronic expansion valve, and other equipment components. The indoor unit included an indoor heat exchanger and control system. The system principle and equipment pictures are shown in Figures 1–3. The total area of the solar energy collector was 10.5 m<sup>2</sup>, and the collector efficiency was more than 55%. The fan airflow was 570 m<sup>3</sup>/h. The refrigerant of the EVI-ASHP system was R32, with a rated heating capacity of 4000 W and a rated power

of 1700 W. The EVI compressor used a fully enclosed DC inverter. Both the indoor and outdoor units of the EVI-ASHP system used fin heat exchangers.



Note on Solar air collector:

- OCA — Outdoor cold air
- C — Collector
- F — Fan
- HU — Heating unit

Note on EVI air source heat pump:

- OHE — Outdoor heat exchanger
- C — Compressor
- FT — Flash tank
- EEV 2 — Electronic expansion valve 2
- FWRV — Four—way reversing valve
- ALS — Air—liquid separator
- EEV 1 — Electronic expansion valve 1
- MFM — Mass flow meter
- HM — Hydraulic mirror
- IHE — Indoor heat exchanger
- FD — Filter dryer

Figure 1. Experimental principles and measurement point layout diagram of the SC-EVIHP system.

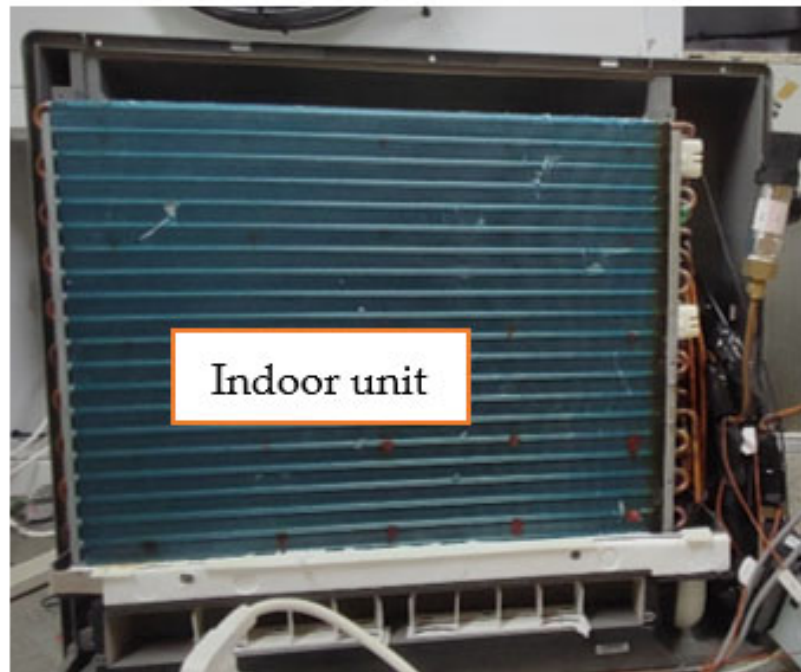
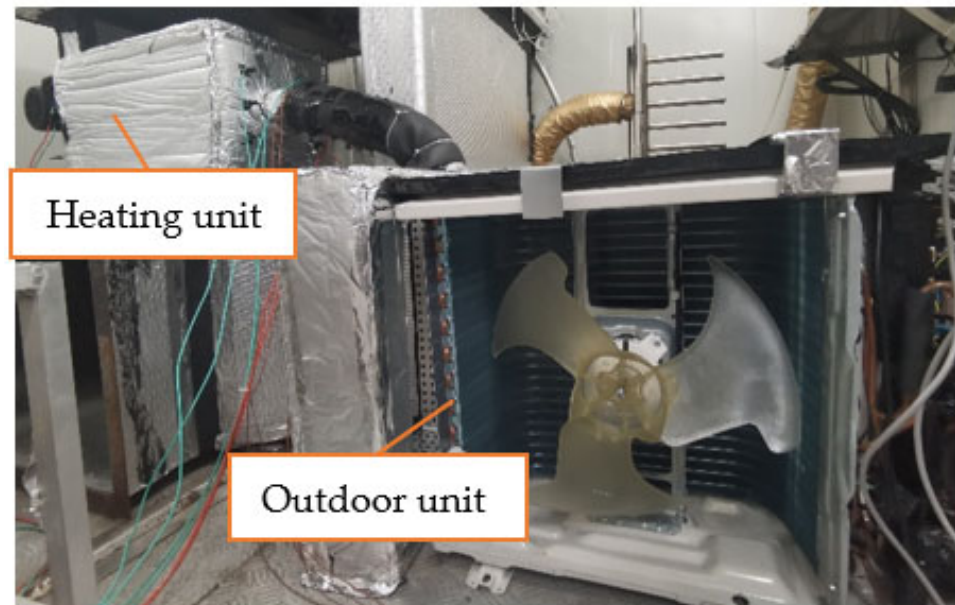


Figure 2. Physical picture of the indoor unit of the SC-EVIHP system.



**Figure 3.** Physical picture of the outdoor unit of the SC-EVIHP system.

The experiment was carried out in an enthalpy difference laboratory, meeting the requirements of relevant national standards. In order to simplify the experiment and operate it easily, TRNSYS software was used to simulate the solar air collector, as shown in Figure 4. Through the software simulation, the outdoor air heated by the solar air collector could be measured. The same effect could be achieved by using the heating device to provide hot air to the same temperature. Eight groups of measuring points were set up on the system to measure the pressure and temperature at each point. The system was equipped with a mass flow meter, a power meter, a hydraulic mirror, a filter drier, and other equipment. The specific experimental equipment parameters are shown in Table 1. An Agilent 34,972 A (Keysight Technologies, Silicon, CA, USA) Valley was used for data collection at an interval of 5 s.

**Table 1.** Experimental instrument parameters.

Testing Instrument	Product Model	Range	Accuracy
T-type thermocouples	SH-T	−99.9~300 °C	±0.15 °C
Diffusible silicon pressure transducer	MIKP300	0–5 MPa	0.25 class
Mass flow meter	RHM18913	0~1.7 kg/s	±0.2%
Three-phase electronic measurement and control meter	TP612	0~756,000 kW	0.5 class
Filter dryer	DFS-083S	-	-
Hydraulic mirror	SYJ6	-	-

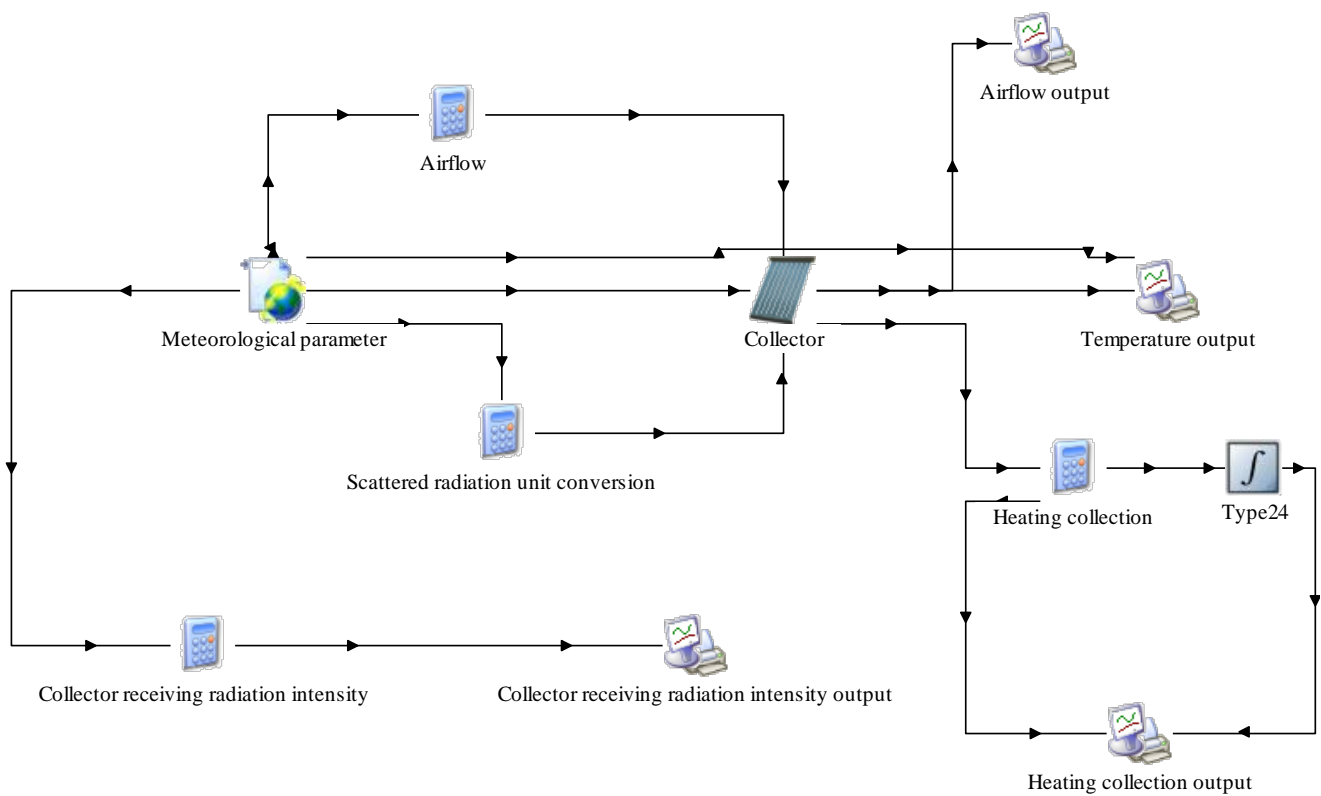


Figure 4. Solar air collector model.

2.2. Thermodynamic Cycle Analysis

Figure 5 shows the pressure enthalpy diagram of the SC-EVIHP system. Generally, the operation process of the heat pump system is 1—2—3—4—1. The heating capacity of the system is improved because more refrigerant in the EVIHP system enters the condenser through the vapor injection loop [8]. The compression process can be divided into three stages: the first stage of compression before the vapor injection (1—9), the middle stage of the vapor injection (7—10, 9—10), and the second stage of compression after the vapor injection (10—11). After the refrigerant in the condenser exchanges heat with the external environment (11—3), the refrigerant is primarily throttled (3—5) into the flash tank, and then the refrigerant is diverted into two routes. Saturated vapor refrigerant directly enters the compressor through the vapor injection loop (5—7—10). The saturated liquid refrigerant enters the evaporator through secondary throttling and then enters the compressor for circulation (6—8—1).

The thermodynamic calculation formula is shown in Formulas (1) and (2):

The heating capacity of the SC-EVIHP system  $\dot{Q}$ :

$$\dot{Q} = (\dot{m} + i) \times (h_{11} - h_3) \tag{1}$$

In Formula (1),  $\dot{m} + i$  is the mass flow through the condenser (kg/s), which is measured by the mass flowmeter.  $h_{11}$  is the enthalpy of the condenser inlet (kJ/kg).  $h_3$  is the enthalpy of the condenser outlet (kJ/kg).

Unit COP:

$$COP = \frac{\dot{Q}}{\dot{W} + \dot{W}_0} \tag{2}$$

In Formula (2),  $\dot{Q}$  is the heating capacity of the heat pump (kW).  $\dot{W}$  is the compressor power (kW), which is measured by a three-phase power meter.  $\dot{W}_0$  is the heater fan power

(kW), which is a CY125 (Shenzhen Xin Hao Long Electronic Technology Co., Ltd, Shenzhen, China) centrifugal fan with a power rating of 108 W.

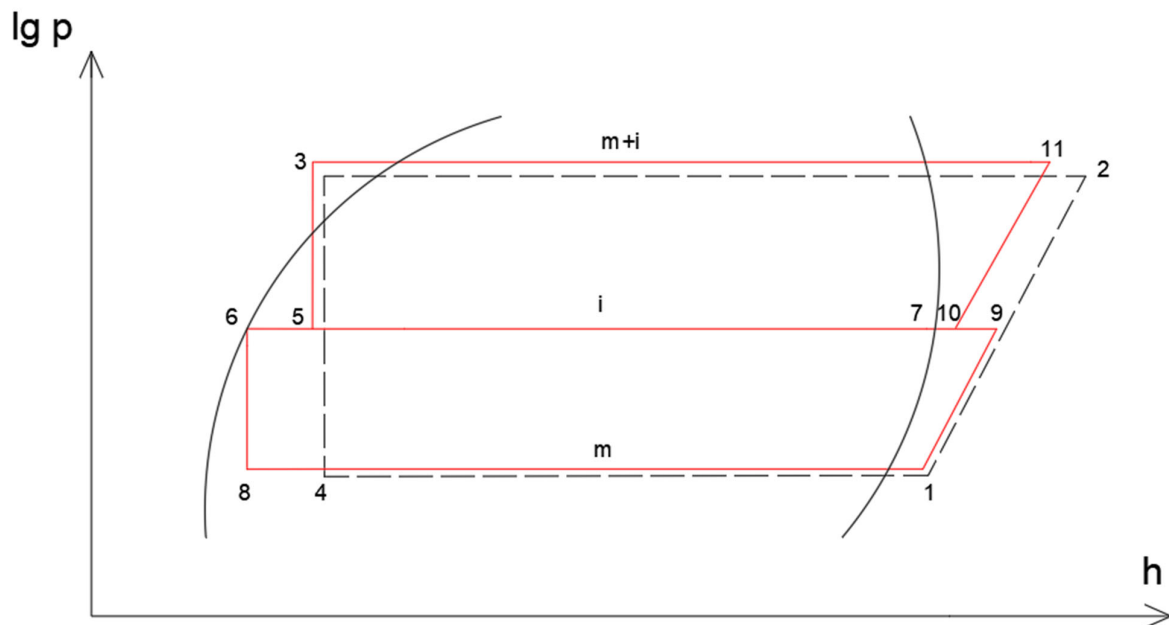


**Figure 5.** Diagram of the pressure enthalpy of the system.

As can be seen from the pressure enthalpy diagram in Figure 5, the total heating capacity of the SC-EVIHP system is:

$$\dot{Q} = (\dot{m} + i)(h_{11} - h_3) = \dot{m}(h_1 - h_8) + \dot{m}(h_9 - h_1) + (\dot{m} + i)(h_{11} - h_{10}) \quad (3)$$

In Formula (3),  $h_i$  is the enthalpy at the corresponding point (kJ/kg).  $\dot{m}(h_1 - h_8)$  is the heat absorption of the refrigerant in the evaporator.  $\dot{m}(h_9 - h_1)$  is the work performed by the primary compression of the compressor.  $\dot{m}(h_{11} - h_{10})$  is the work performed by the secondary compression of the compressor.

The heating capacity of the ASHP system without a flash tank is:

$$\dot{Q}_1 = \dot{m}(h_1 - h_4) + \dot{m}(h_2 - h_1) \quad (4)$$

According to (3) and (4), the difference between the two is the increase in the heating capacity of the ASHP system with flash tank. It is as follows:

$$\Delta\dot{Q} = \dot{m}(h_4 - h_8) + (\dot{m} + i)(h_{11} - h_{10}) - \dot{m}(h_2 - h_9) \quad (5)$$

According to the analysis of Formula (5), the heating capacity increment of the SC-EVIHP system comes from the supercooling of the refrigerant inside the flash tank and the increased work consumption of the compressor through the vapor injection loop.

### 3. Experimental Scheme Design

#### 3.1. Performance Analysis of the SC-EVIHP System for a Typical-Weather Day

The temperature data for typical meteorological days in winter was simulated using TRNSYS software in Harbin, China. The result is shown in Figure 6. The temperature data were selected for experiments to test the heating performance of the SC-EVIHP system in cold areas. According to the requirements, the indoor temperature of the enthalpy difference laboratory was controlled at 14 °C. The experiment was divided into two groups. One group was the performance analysis of the EVI-ASHP system without the solar air collector. The second group was the performance analysis experiment of the SC-EVIHP system with the solar air collector. The operational performance of the SC-EVIHP system was investigated through comparative experiments.

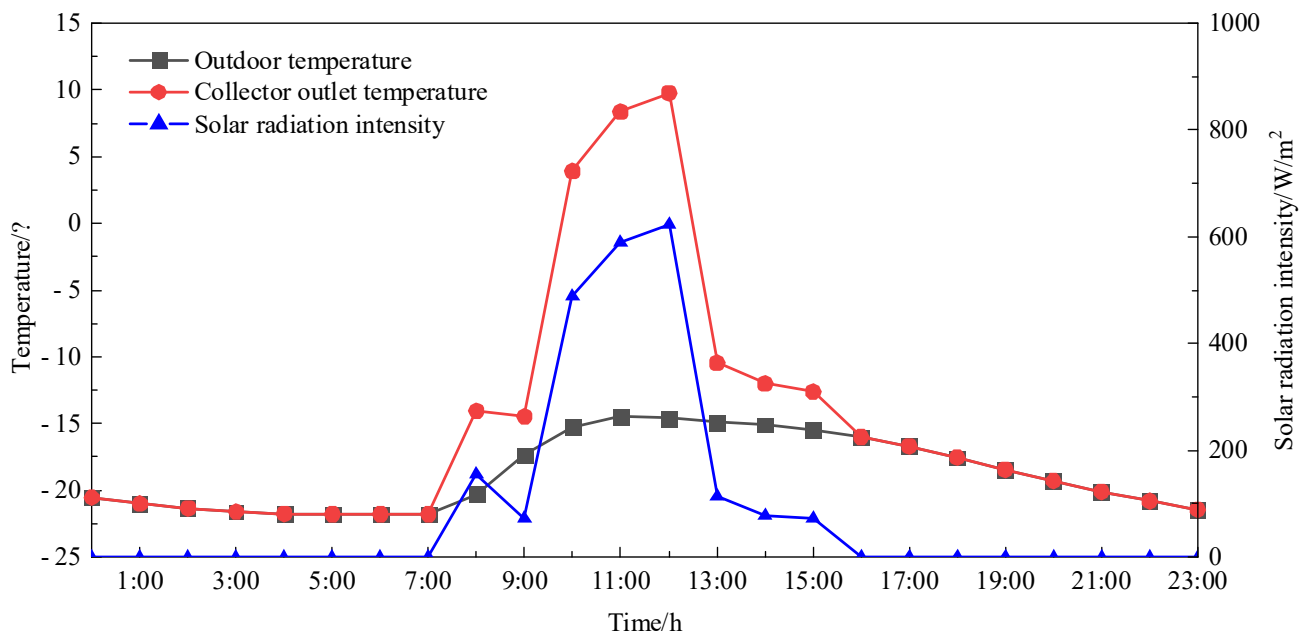


**Figure 6.** The import and export temperature and solar radiation intensity for typical meteorological solar collectors in winter in Harbin.

### 3.2. Study of the Operational Regulation of the SC-EVIHP System

In order to further explore the operational characteristics of the SC-EVIHP system, test conditions were formulated according to the standards as shown in Table 2. First, the system was tested without the solar air collector to measure heating capacity, power consumption, and other performance parameters. Hot air with different temperatures was blown to the outdoor unit through the heating device. The airflow of the heating device was set at  $200 \text{ m}^3/\text{h}$  to explore the operational regulations of the SC-EVIHP system under different outdoor temperatures.

**Table 2.** Test conditions.

	Indoor Side		Outdoor Side		
Dry-bulb temperature/ $^{\circ}\text{C}$	20	−20	−12	−5	7
Wet-bulb temperature/ $^{\circ}\text{C}$	15	-	−13.5	−1	6

## 4. Experimental Results and Analysis

### 4.1. Experimental Study of the SC-EVIHP System on a Typical-Weather Day in Winter

Figures 7 and 8 show the comparison between the heating capacity and COP of the system. As can be seen from the figures, when the solar radiation intensity was 0, the heating capacity and COP of the two systems were the same. During 7:00~16:00, the solar radiation intensity increased first and then decreased to 0. Because the conventional EVI-ASHP system has no solar air collector, system performance was mainly affected by the outdoor temperature. At this point, the heating capacity and COP were low. For the SC-EVIHP system, the hot-air temperature at the solar air collector outlet increased rapidly with the increase in solar radiation intensity. The evaporation temperature of the SC-EVIHP system increased. This made the suction gas capacity of the compressor smaller and the mass flow of the heat pump moving fluid larger, thus causing an increase in the heating capacity and COP of the system. During this period, the heating capacity increased by 2.3~24.9%, with an average increase of 9.2%. The COP increased by 0.59~12.53%, with an average increase of 5.6%. At 12:00, the solar radiation intensity was the highest. The heating capacity and COP of the SC-EVIHP system also reached their peak. At this point, the heating capacity was 4.16 kW and the COP was 2.35. Compared with the EVI-ASHP

system, the heating capacity and COP were increased by 24.9% and 12.5%, respectively. According to the experimental data, compared with the single EVI-ASHP system, the SC-EVIHP system had a better heating effect and more energy conservation. From 12:00 to 13:00, due to the sudden decrease in solar radiation intensity, the heating capacity and COP of the SC-EVIHP system also decreased. This indicates that the SC-EVIHP system is greatly affected by solar radiation intensity.

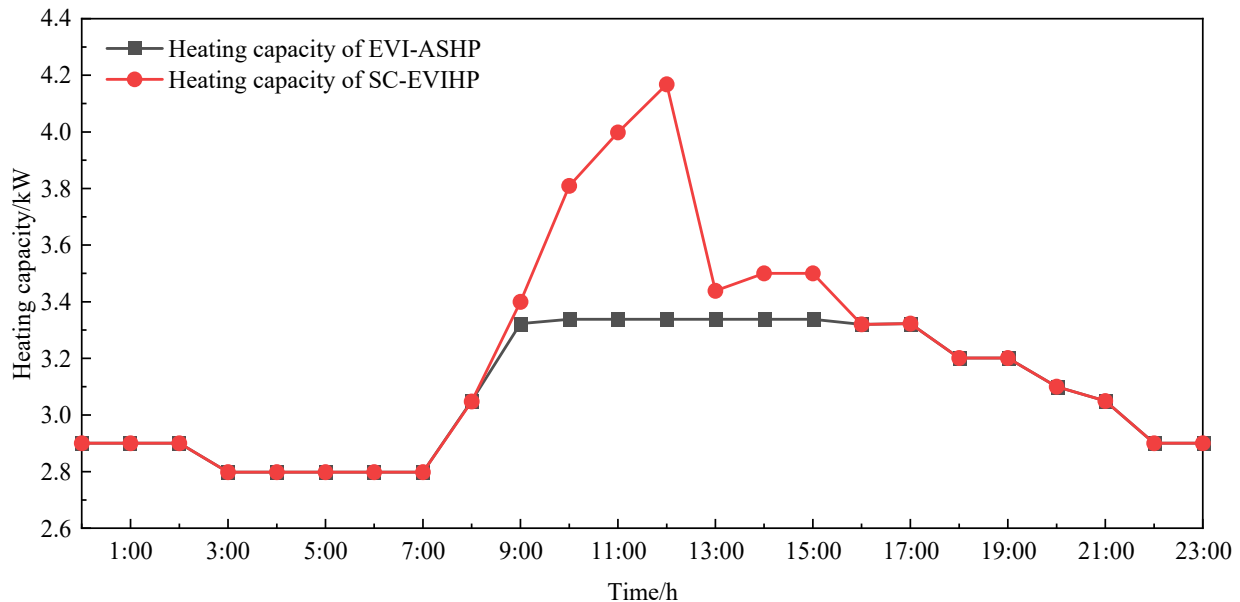


Figure 7. Comparison of heating capacity of the systems.

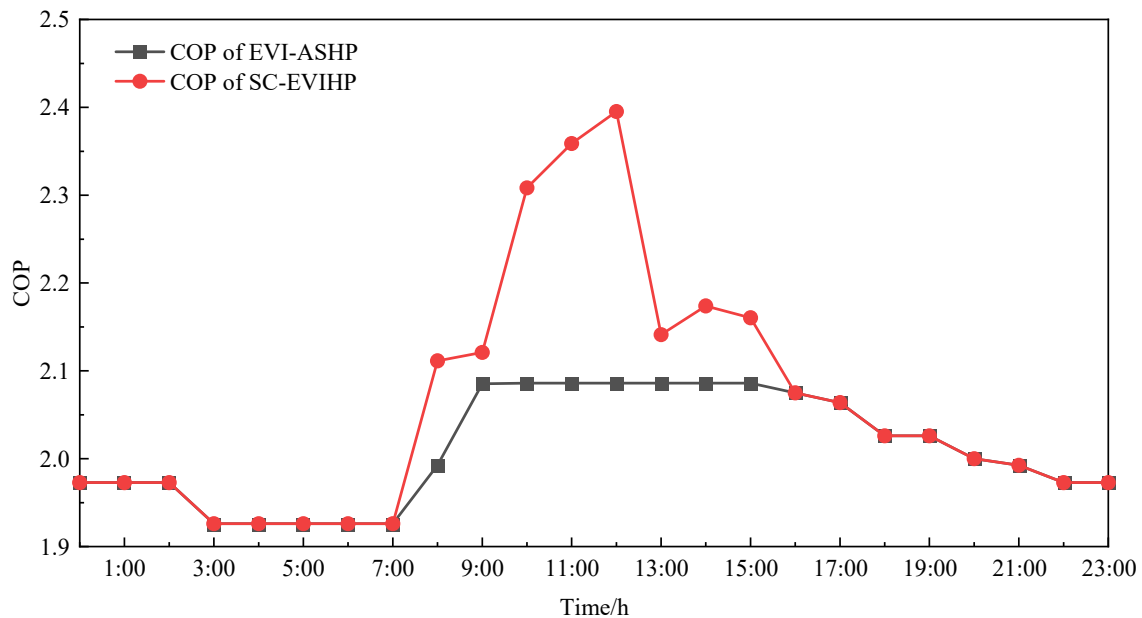


Figure 8. Comparison of COP of the systems.

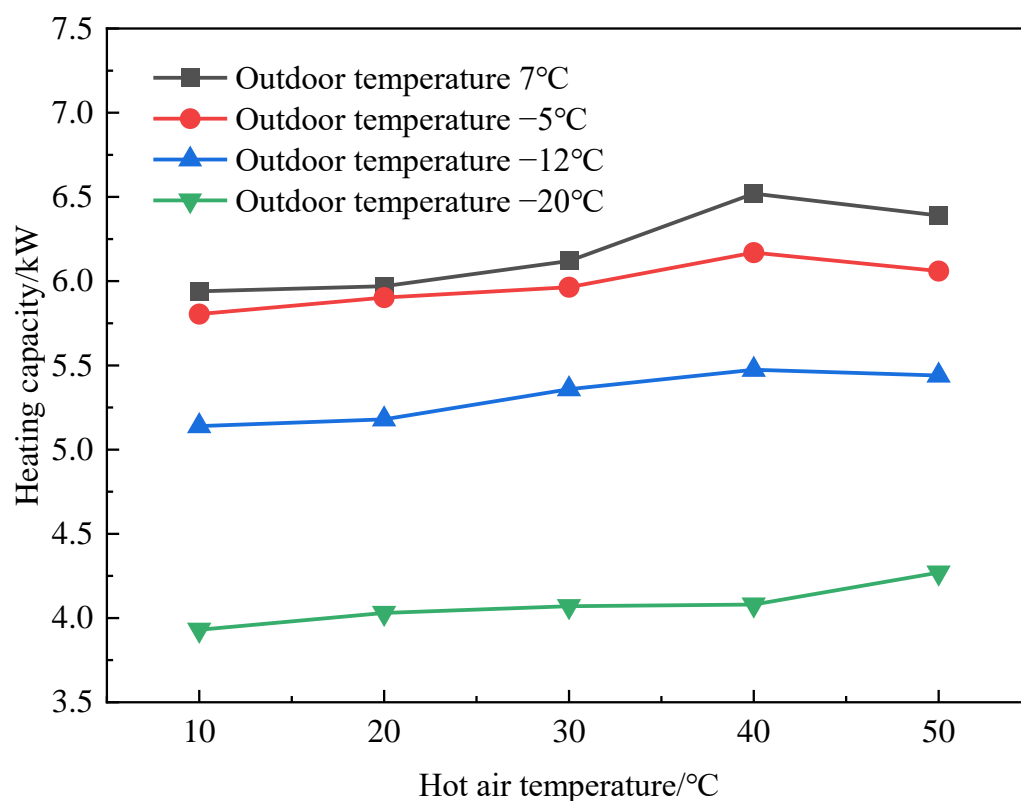
#### 4.2. Study of Operational Performance of the SC-EVIHP System

Table 3 shows the operational performance of the EVI-ASHP system at different outdoor temperatures. It can be seen that both the heating capacity and COP of the system decreased with the fall of outdoor temperatures. They decreased by 66.4% and 22.3%, respectively, which indicates that the system was greatly affected by the outdoor environment.

**Table 3.** Operational performance of the EVI-ASHP system at different outdoor temperatures.

Outdoor Temperature/°C	Indoor Temperature/°C	Heating Capacity/kW	Power Consumption/kW	COP
−20	20	3.90	1.70	2.29
−12	20	5.11	2.03	2.52
−5	20	5.56	2.10	2.65
7	20	6.49	2.32	2.80

The comparable results of the heating capacity of the SC-EVIHP system under different outdoor temperatures and different hot air temperatures are displayed in Figure 9. As shown in Figure 9, when the outdoor temperature was  $-12\text{ }^{\circ}\text{C}$ ,  $-5\text{ }^{\circ}\text{C}$ , and  $7\text{ }^{\circ}\text{C}$ , respectively, the heating capacity increased first and then decreased with the increase in hot air temperature. When the hot air temperature was  $40\text{ }^{\circ}\text{C}$ , the heating capacity reached the maximum value, then it decreased with the rising hot air temperature. The reason for this is that with the increase in hot air temperature, the evaporation temperature of the system rose gradually, and more refrigerant absorbed heat from the outside to evaporate for circulation, thus the heating capacity of the system increased. However, as the hot air temperature continued to rise, more refrigerant entered the compressor through the vapor injection loop, causing a decrease in exhaust temperature and the temperature of the condenser inlet. These results caused a decrease in the heat transfer temperature difference between the system and the external environment. Although the mass flow in the system was improved, the heat transfer temperature difference plays a dominant role in the heat transfer process, so the heating capacity decreased. When the outdoor temperature was  $-20\text{ }^{\circ}\text{C}$ , the heating capacity gradually increased with the rising hot air temperature. The heating capacity can be kept at about 4 kW. This indicates that a good heating condition can still be achieved in a cold area. As can be seen from Figure 9, as the outdoor ambient temperature decreased, the heating capacity of the SC-EVIHP system had greater improvement [22,23].

**Figure 9.** Heating capacity of the SC-EVIHP system.

Comparison of the COP of the SC-EVIHP system at different outdoor temperatures and different hot air temperatures is shown in Figure 10. The variation trend of the COP was similar to that of the heating capacity. When the outdoor temperature was  $-12\text{ }^{\circ}\text{C}$ ,  $-5\text{ }^{\circ}\text{C}$ , and  $7\text{ }^{\circ}\text{C}$ , respectively, the COP increased first and then decreased with the increase in hot air temperature. When the hot air temperature was  $40\text{ }^{\circ}\text{C}$ , the COP reached the maximum value, then it decreased with the rising hot air temperature. The reason is that with the increase in hot air temperature, the evaporation temperature of the system rose gradually, thus causing the heating capacity of the system to increase. However, as the hot air temperature continued to rise, the heating capacity of the system decreased. Moreover, as more refrigerant entered circulation, the power consumption of the compressor also increased. This resulted in a decrease in COP. When the outdoor temperature was  $-20\text{ }^{\circ}\text{C}$ , the COP gradually increased with the increasing hot air temperature. This indicates that the SC-EVIHP system operates more stably in cold regions.

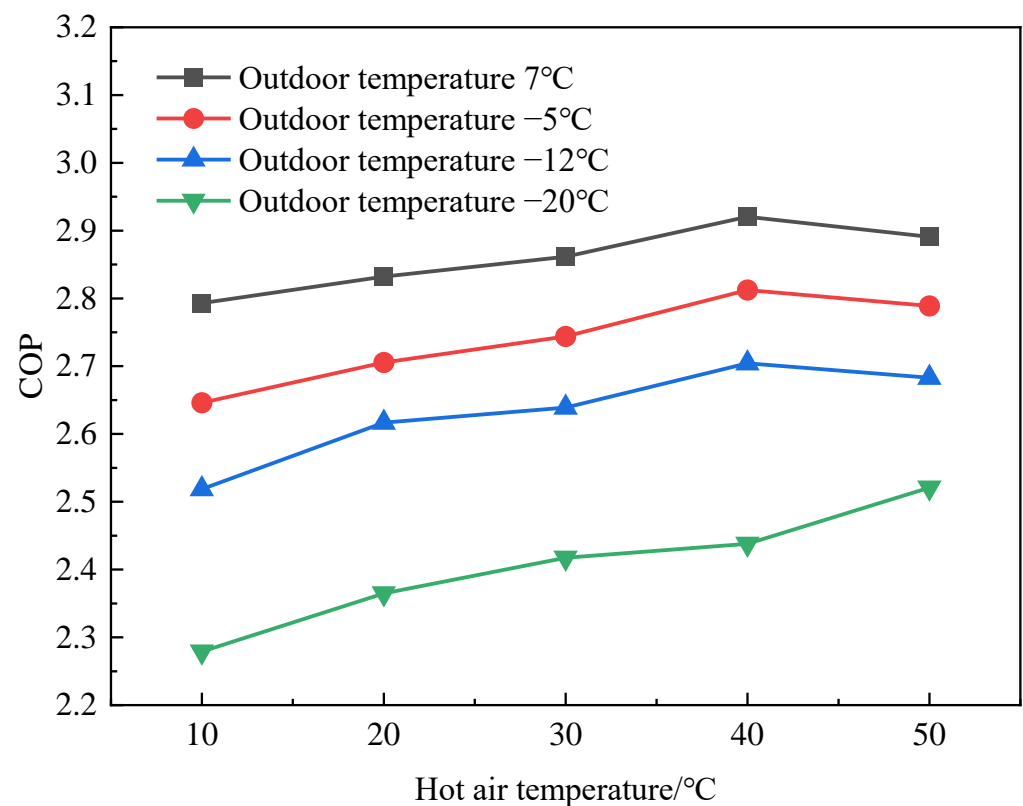


**Figure 10.** COP of the system.

As can be seen from Figures 9 and 10, when the airflow and the hot air temperature were  $200\text{ m}^3/\text{h}$  and  $40\text{ }^{\circ}\text{C}$ , respectively, the performance of the SC-EVIHP system was the best. When the outdoor environment is extremely cold, the hot air temperature can be continuously increased to improve the performance of the SC-EVIHP system.

The comparison of compressor exhaust pressure of the SC-EVIHP system at different outdoor temperatures and different hot air temperatures is shown in Figure 11. The compressor exhaust pressure was greatly affected by the outdoor temperature. The exhaust pressure increased with the increasing outdoor temperature. When the outdoor temperature was unchanged, the exhaust pressure gradually decreased by 7.5 to 12.1% as the hot air temperature increased. When the outdoor temperature was  $-20\text{ }^{\circ}\text{C}$ , the decrease range was the largest. This indicates that the SC-EVIHP system has its best operational performance in a low-temperature environment.

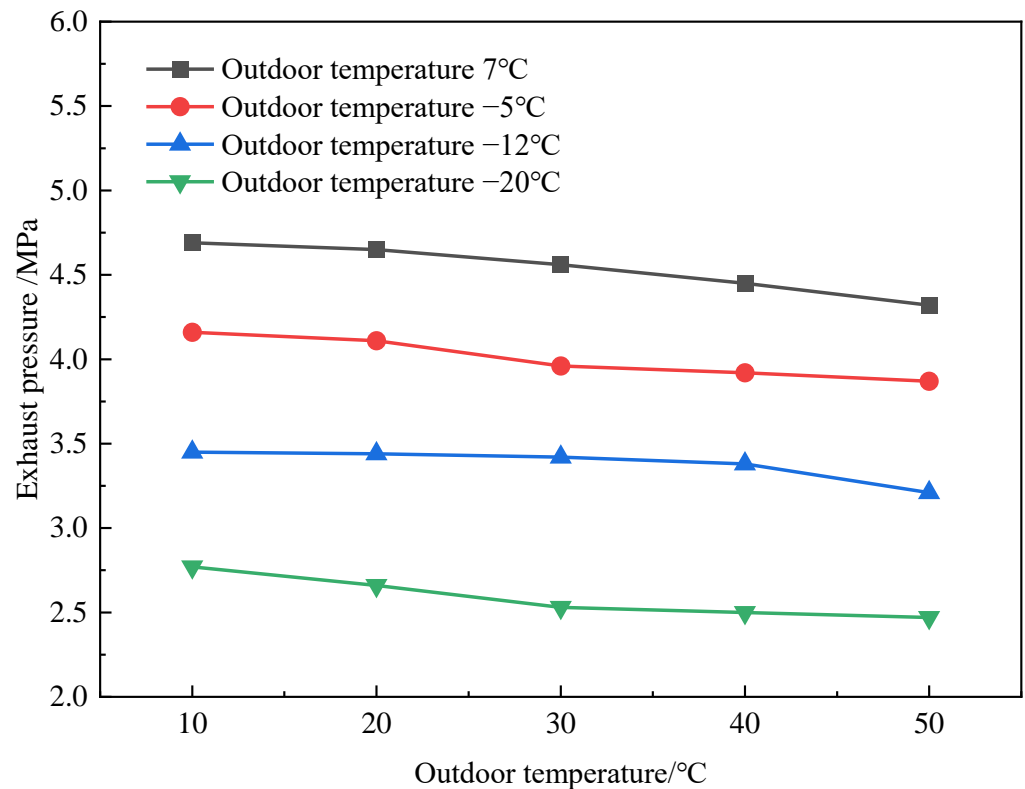


**Figure 11.** Compressor exhaust pressure changes under different operational conditions.

Figure 12 shows the comparison of compressor exhaust temperatures of the SC-EVIHP system at different outdoor temperatures and different hot air temperatures. Compressor exhaust temperature is mainly affected by two parameters: suction temperature and compression ratio. As the outdoor temperature increased, the evaporation temperature increased, causing the compressor suction temperature to rise and the compression ratio to decrease. At this time, the suction temperature plays a leading role in causing the rise of the compressor exhaust temperature. As shown in Figure 12, when the outdoor temperature was 7 °C, the compressor exhaust temperature was 131 °C. High compressor exhaust temperature causes carbonization of the lubricating oil. It will increase the wear of the compressor's moving parts, thus affecting the service life of the compressor. As the hot airflow increased, more refrigerant entered the compressor from the vapor injection loop. The compressor exhaust temperature was effectively decreased by 9~21%. This shows that the SC-EVIHP system is safer and more stable than the EVI-ASHP system.

It can be seen from Figures 13 and 14 that the heating capacity and COP of the SC-EVIHP system at different temperatures were improved with hot air. The heating capacity of the SC-EVIHP system improved by 3.9~10.9% and the COP improved by 6.1~11.1%. When the outdoor temperature was -5 °C, the maximum increase in heating capacity was 10.9% compared with the EVI-ASHP system. When the outdoor temperature was -12 °C, the COP reached its maximum increase of 11.1%. When the outdoor temperature was -20 °C, the COP of the SC-EVIHP system still increased by 10%. This indicates that the SC-EVIHP system is more suitable and energy-saving in cold areas.

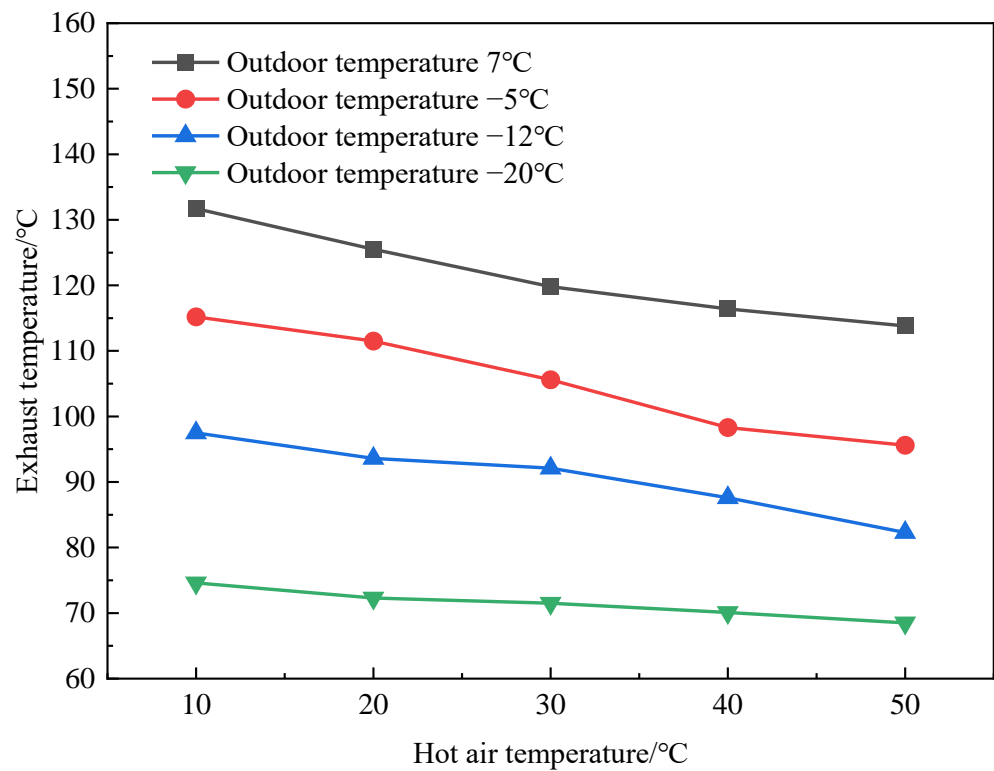


Figure 12. Compressor exhaust temperature changes under different operational conditions.

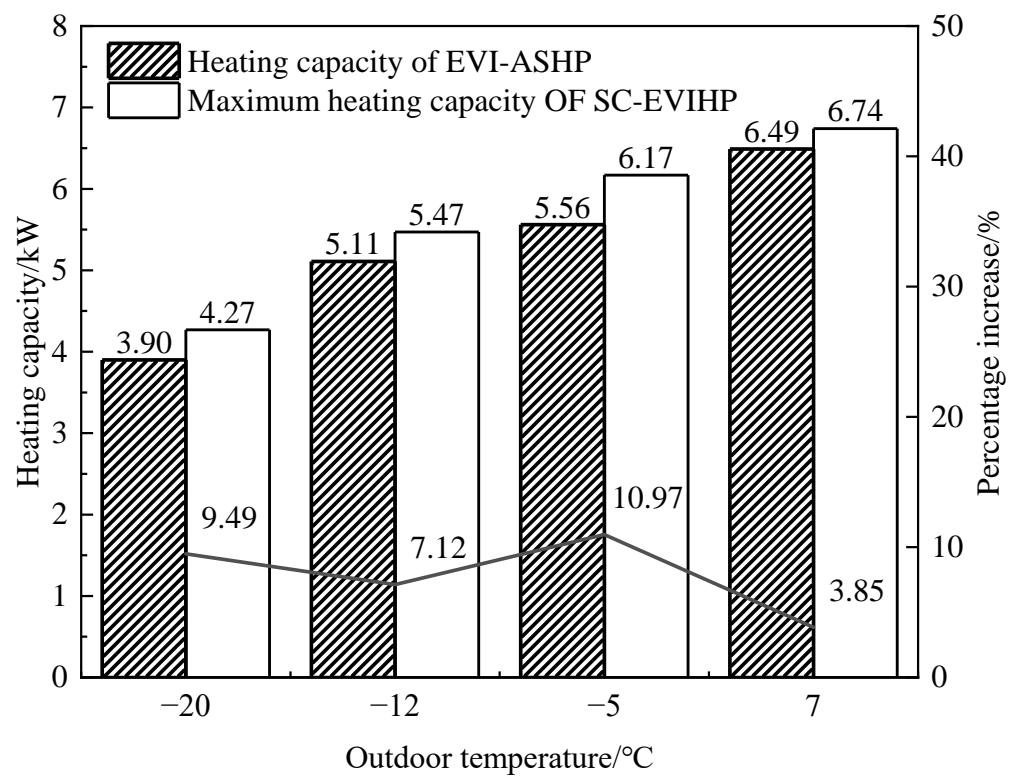


Figure 13. Heating capacity comparison at different outdoor temperatures.

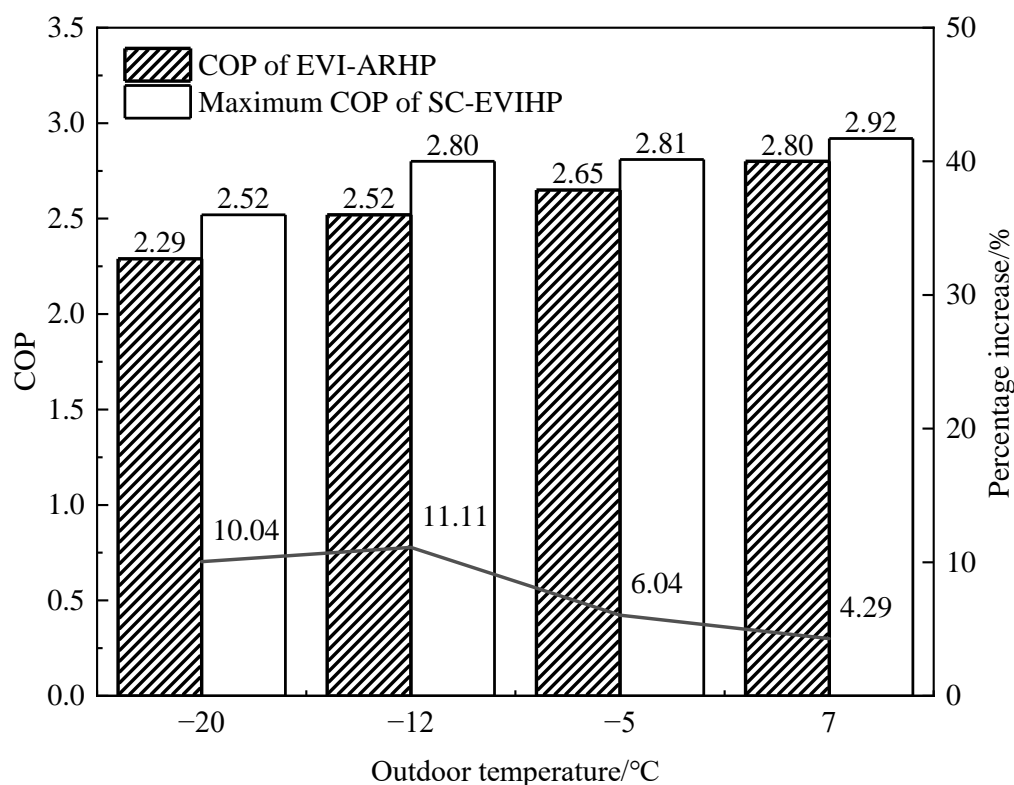


Figure 14. COP comparison under different outdoor temperatures.

### 5. Economic Analysis

The initial investment, labor cost, and operational cost of the SC-EVIHP system and EVI-ASHP system are analyzed and compared in Table 4. According to the survey, the initial investment for a conventional EVI-ASHP system is about USD 630. The investment for a solar air collector is USD 560. The SC-EVIHP system is relatively complex, so the labor cost is USD 140. The labor cost of a conventional EVI-ASHP system is USD 70. Taking Harbin as the research city, the average power used by the SC-EVIHP system was 2 kW and the average power used by the conventional EVI-ASHP system was 3.1 kW. The unit electricity price in Harbin is 0.0714 USD /kWh. The daily operational time of the two systems was 8 h. During the six-month heating period, the annual operating cost of the SC-EVIHP system was USD 201.6, while the conventional EVI-ASHP was USD 312.48. According to the analysis, although the initial investment of the SC-EVIHP system is relatively high, its operational cost is significantly lower. The economic advantages of the SC-EVIHP system will become more apparent with increased years of operation. Assuming that the service life of the two systems is 15 years, the SC-EVIHP system can save the user USD 1663.2 in terms of electricity costs. The SC-EVIHP system is stable and reliable in operation, with outstanding energy-saving effects and obvious economic advantages. It will have broad application prospects.

Table 4. Economic benefit analysis.

	SC-EVIHP System	Conventional EVI-ASHP System
Initial equipment Investment/USD	1190	560
Labor cost/USD	140	70
Annual operating cost/USD	201.6	312.5

## 6. Conclusions

Through the exploration of the operational regulation of the SC-EVIHP system, the experimental results are as follows:

- (1) The SC-EVIHP system is greatly affected by solar radiation intensity. In the experiment regarding a typical meteorological day in winter, the maximum outlet temperature of the solar air collector appeared at 12 o'clock; at this time, the heating capacity and COP of the SC-EVIHP system were reaching their maximum value. Compared with the conventional EVI-ASHP system, the heating capacity and COP of the SC-EVIHP system were improved by 24.9% and 12.5%, respectively.
- (2) In the conditions using hot air at different temperatures, the heating capacity and COP of the SC-EVIHP system increased by 3.9~10.9% and 6.1~11.1%, respectively. When the outdoor temperature was  $-12\text{ }^{\circ}\text{C}$  and the hot air temperature was  $40\text{ }^{\circ}\text{C}$ , the COP of the SC-EVIHP system increased by 11.1% at most and still increased by 10% at the extreme outdoor temperature of  $-20\text{ }^{\circ}\text{C}$ .

This research improves the heating performance of the EVIHP system and has very broad application prospects in cold regions. However, some improvements can be made to this system. It can adopt a solar air collector with energy storage materials to extend the operational hours of the system at night. Furthermore, suitable control schemes and optimized air supply mode can be researched to optimize the overall performance of the system.

**Author Contributions:** Investigation, Y.P.; data curation, Y.D.; writing—original draft preparation, Z.L.; writing—review and editing, F.Z.; visualization, Y.Z.; project administration, Z.M. All authors have read and agreed to the published version of the manuscript.

**Funding:** This work is supported by a sub-project of the National Key Point Research and Invention Program of the thirteenth (2018YFD1100705-04) key research and development project of Henan Province in 2022 (221111320200), young teacher support of Zhongyuan University of Technology (2020XQG05).

**Data Availability Statement:** Not applicable.

**Conflicts of Interest:** The authors declare no conflict of interest.

## References

1. Wang, Y.; Rao, Z.; Liu, J.; Liao, S. An optimized control strategy for integrated solar and air-source heat pump water heating system with cascade storage tanks. *Energy Build.* **2020**, *210*, 109766. [[CrossRef](#)]
2. Huang, S.; Zuo, W.; Lu, H.; Liang, C.; Zhang, X. Performance comparison of a heating tower heat pump and an air-source heat pump: A comprehensive modeling and simulation study. *Energy Convers. Manag.* **2019**, *180*, 1039–1054. [[CrossRef](#)]
3. Fan, Y.; Li, J.; Zhao, X.; Myers, S.; Cheng, Y.; Yu, M.; Akhlaghi, Y.G.; Ma, X.; Yu, S. A proof-of-concept study of a novel ventilation heat recovery vapour injection air source heat pump. *Energy Convers. Manag.* **2022**, *256*, 115404. [[CrossRef](#)]
4. Zhu, J.H.; Sun, Y.Y.; Wang, W.; Deng, S.M.; Ge, Y.J.; Li, L.T. Developing a new frosting map to guide defrosting control for air-source heat pump units. *Appl. Therm. Eng.* **2015**, *90*, 782–791. [[CrossRef](#)]
5. Wang, W.; Feng, Y.C.; Zhu, J.H.; Li, L.T.; Guo, Q.C.; Lu, W.P. Performances of air source heat pump system for a kind of mal-defrost phenomenon appearing in moderate climate conditions. *Appl. Energy* **2013**, *112*, 1138–1145. [[CrossRef](#)]
6. Wang, W.; Xiao, J.; Guo, Q.C.; Lu, W.P.; Feng, Y.C. Field test investigation of the characteristics for the air source heat pump under two typical mal-defrost phenomena. *Appl. Energy* **2011**, *88*, 4470–4480. [[CrossRef](#)]
7. Yan, G.; Bai, T.; Yu, J. Energy and exergy efficiency analysis of solar driven ejector-compressor heat pump cycle. *Sol. Energy* **2016**, *125*, 243–255. [[CrossRef](#)]
8. Jie, X.; Xianmin, G.; Liping, X. Experimental Study on Performance of Flash-tank Vapor Injection Air-Source Heat Pump System with Refrigerant R32. *Energy Procedia* **2017**, *142*, 950–956. [[CrossRef](#)]
9. Han, X.; Zou, H.; Kang, W.; Xu, H.; Chen, Y.; Tian, C. Experimental investigation on vapor injection ASHP for electric rail vehicles in cold region. *Appl. Therm. Eng.* **2019**, *153*, 473–482. [[CrossRef](#)]
10. Wei, W.; Ni, L.; Dong, Q.; Wang, W.; Ye, J.; Xu, L.; Yang, Y.; Yao, Y. Experimental investigation on improving defrosting performance of air source heat pump through vapor injection. *Energy Build.* **2022**, *256*, 111696. [[CrossRef](#)]
11. Heo, J.; Kang, H.; Kim, Y. Optimum cycle control of a two-stage injection heat pump with a double expansion sub-cooler. *Int. J. Refrig.* **2012**, *35*, 58–67. [[CrossRef](#)]

12. Wang, J.; Qv, D.; Yao, Y.; Ni, L. The difference between vapor injection cycle with flash tank and intermediate heat exchanger for air source heat pump: An experimental and theoretical study. *Energy* **2021**, *221*, 119796. [[CrossRef](#)]
13. Li, W.; Liu, R.; Liu, Q.; Liu, Y.; Wang, D.; Xia, S.; Shi, J.; Chen, J. Upstream and downstream injection effects on R134a economized vapor injection heat pump system at low temperatures for electric vehicles. *Int. J. Refrig.* **2020**, *120*, 1–11. [[CrossRef](#)]
14. Jia, S.; Shan, S.; Zhang, F.; Liu, B.; Zhang, Q.; Zhou, Z. Parametrical analysis of a novel CHP system based on solar-gas assisted thermo-photovoltaic device. *Energy Convers. Manag.* **2022**, *271*, 116316. [[CrossRef](#)]
15. Wang, D.; Chen, R.; Zhou, Y.; Wang, Y.; Liu, Y. Optimization and techno-economic analysis of combined gas-fired boiler and solar heating system for capacity-increase cities. *Sol. Energy* **2022**, *243*, 225–235. [[CrossRef](#)]
16. Aligholami, M.; Khosroshahi, S.S.; Khosroshahi, A.R. Hydrodynamic and thermodynamic enhancement of a solar chimney power plant. *Sol. Energy* **2019**, *191*, 180–192. [[CrossRef](#)]
17. Yang, L.W.; Hua, N.; Pu, J.H.; Xia, Y.; Zhou, W.B.; Xu, R.J.; Yang, T.; Belyayev, Y.; Wang, H.S. Analysis of operation performance of three indirect expansion solar assisted air source heat pumps for domestic heating. *Energy Convers. Manag.* **2022**, *252*, 115061. [[CrossRef](#)]
18. Wang, Z.; Chen, H.; Sun, X.; Lu, H.; Wang, T. Optimizing the solar-air hybrid source heat pump heating system based on the particle swarm algorithm. *Energy Rep.* **2022**, *8*, 379–393. [[CrossRef](#)]
19. Long, J.; Xia, K.; Zhong, H.; Lu, H.; Yongga, A. Study on energy-saving operation of a combined heating system of solar hot water and air source heat pump. *Energy Convers. Manag.* **2021**, *229*, 113624. [[CrossRef](#)]
20. Xu, W.; Liu, C.; Li, A.; Li, J.; Qiao, B. Feasibility and performance study on hybrid air source heat pump system for ultra-low energy building in severe cold region of China. *Renew. Energy* **2020**, *146*, 2124–2133. [[CrossRef](#)]
21. Januševičius, K.; Streckienė, G.; Bielskus, J.; Martinaitis, V. Validation of unglazed transpired solar collector assisted air source heat pump simulation model. *Energy Procedia* **2016**, *95*, 167–174. [[CrossRef](#)]
22. Xu, S.; Niu, J.; Cui, Z.; Ma, G. Experimental research on vapor-injected heat pump using injection subcooling. *Appl. Therm. Eng.* **2018**, *136*, 674–681. [[CrossRef](#)]
23. Yu, M.; Yu, J. Thermodynamic analyses of a solar assisted ejector enhanced vapor injection cycle with subcooler for heat pump dryer application. *Sol. Energy* **2022**, *232*, 376–387. [[CrossRef](#)]